List of Supplementary Materials

1. Figure S1. LN stromal populations remain Kaede Red^+ after photoconversion.
2. Figure S2. ILCs continuously traffic into LNs with different kinetics to T cells.
3. Figure S3. Photoconversion does not cause an increase in the number of ILCs within the labelled bLN.
4. Figure S4. Expression of $S1P_1$ by ILC subsets in the bLN.
5. Figure S5. Treatment with FTY720 results in ILC accumulation within the bLN.
6. Figure S6. Analysis of S1PR expression by ILCs.
7. Figure S7. Identification of ILC subsets within the bLN.
8. Figure S8. Analysis of ILC residency in LNs using H2B-Dendra2 mice.
9. Figure S9. Differences in Dendra Red expression by ILC2s dependent upon identification by transcription factor or cell surface marker expression.
10. Figure S10. Expression of Ki-67 by ILC subsets within the bLN.
11. Figure S11. Comparison of ILC1 and NK cell recirculation through peripheral lymph nodes.
12. Figure S12. Induction of atopic dermatitis causes an increase in the frequency of ILC2s in ear skin.
13. Figure S13. CCR6 is expressed by all ILC subsets in the ear and auLN.
14. Table S1. Raw data.

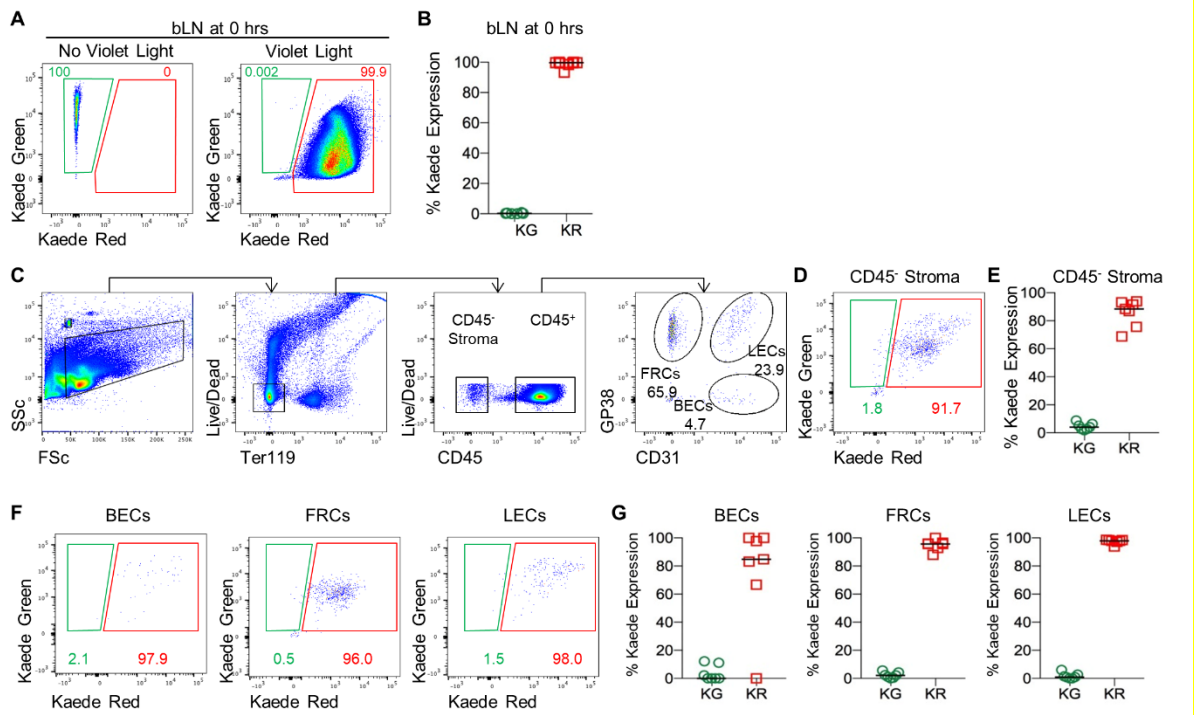

Figure S1. LN stromal populations remain Kaede Red$^+$ after photoconversion. To assess the migratory kinetics of different cellular populations within peripheral LNs, the bLN of Kaede mice was photoconverted and analyzed 72 hrs later. (**A**) Expression of Kaede Green and Kaede Red protein by CD45$^+$ cells isolated from the bLN without (left panel) or immediately after (right panel) photoconversion. (**B**) Percentage of CD45$^+$ cells in the bLN expressing Kaede Green (KG) and Kaede Red (KR) protein immediately after photoconversion (n=8). To assess a non-migratory cell population within the LN, the bLN was photoconverted and the stroma analyzed at 72 hrs post photoconversion. (**C**) Flow cytometry plots identifying stromal cells within the bLN, with blood endothelial cells (BECs), fibroblastic reticular cells (FRCs) and lymphatic endothelial cells (LECs) identified using GP38 versus CD31 expression. (**D**) Kaede Green versus Kaede Red expression by total CD45$^-$ stroma. (**E**) Percentage of stromal cells expressing Kaede Green or Kaede Red (n=7). (**F**) Representative Kaede Green versus Kaede Red expression by BECS, FRCs and LECs. (**G**) Percentage of BECs, FRCs and LECs expressing Kaede Green or Kaede Red (n=7). Data are pooled from a minimum of 2 independent experiments. Values on flow cytometry plots represent percentages; bars on scatter plots represent the median.

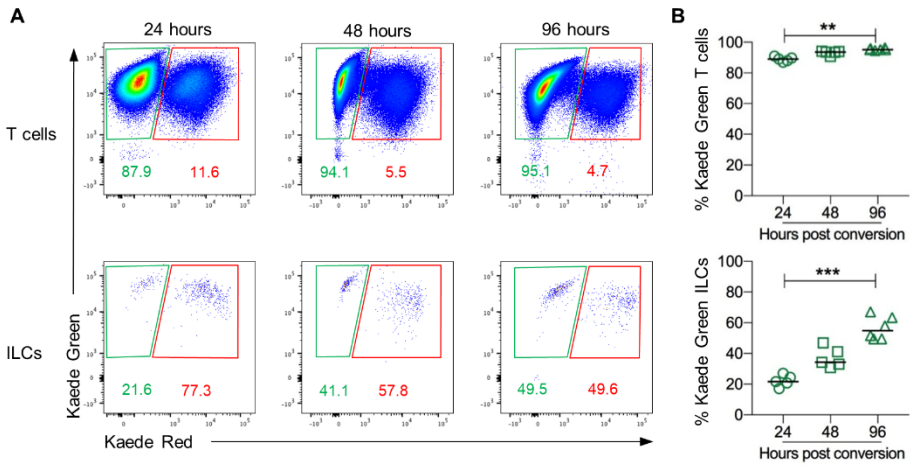

Figure S2. ILCs continuously traffic into LNs with different kinetics to T cells.
To further understand the kinetics of ILC migration through LNs, photoconverted bLNs were analysed at multiple time points post labelling and ILC and T cell populations compared for expression of Kaede Red and Kaede Green protein. (**A**) Expression of Kaede Green and Kaede Red protein by T cells ($CD3^+CD45^+$, upper panels) and ILC ($CD45^+IL\text{-}7R\alpha^+$ Lin{B220, CD11b, CD11c, CD3, CD5, CD19, Ter119, Gr1, CD49b, F4/80, $Fc\varepsilon RI\}^-$, lower panels) isolated from the bLN at different times post photoconversion. (**B**) Percentage of Kaede $Green^+$ T cells (upper panel) and ILC (lower panel) at 24hrs (n=5), 48hrs (n=5) and 96hrs (n=6) post photoconversion. Data are pooled from 2 independent experiments. Values on flow cytometry plots represent percentages; bars on scatter plots represent the median. Statistical significance was tested using an unpaired, non-parametric, Mann-Whitney two-tailed U test: *p≤0.05, **p≤0.01, ***p≤0.001.

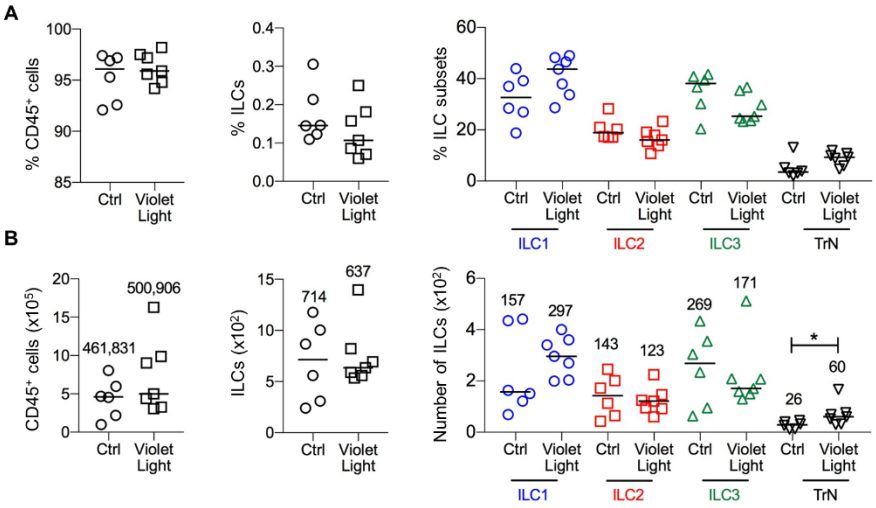

Figure S3. Photoconversion does not cause an increase in the number of ILCs within the labelled bLN.
To determine the effect of the surgical process and photoconversion, the cellularity and ILC composition of the bLN in WT control mice was compared with that of mice that underwent surgery (skin incision and exposure to violet light). (**A**) Percentage of $CD45^+$ cells, ILCs ($CD45^+IL\text{-}7R\alpha^+Lin$ {B220, CD11b, CD11c, CD3, CD5, CD19, Ter119, Gr1, CD49b, F4/80, FcεRI}$^-$) and ILC subsets (identified by transcription factor expression) in control mice (n=6) and surgery ('violet light') mice (n=7). (**B**) Total number of $CD45^+$ cells, ILCs, and ILC subsets in control mice (n=6) and surgery ('violet light') mice (n=7). Data are pooled from 2 independent experiments. Values on flow cytometry plots represent percentages; bars on scatter plots represent the median. Statistical significance was tested using an unpaired, non-parametric, Mann-Whitney two-tailed U test: *p≤0.05.

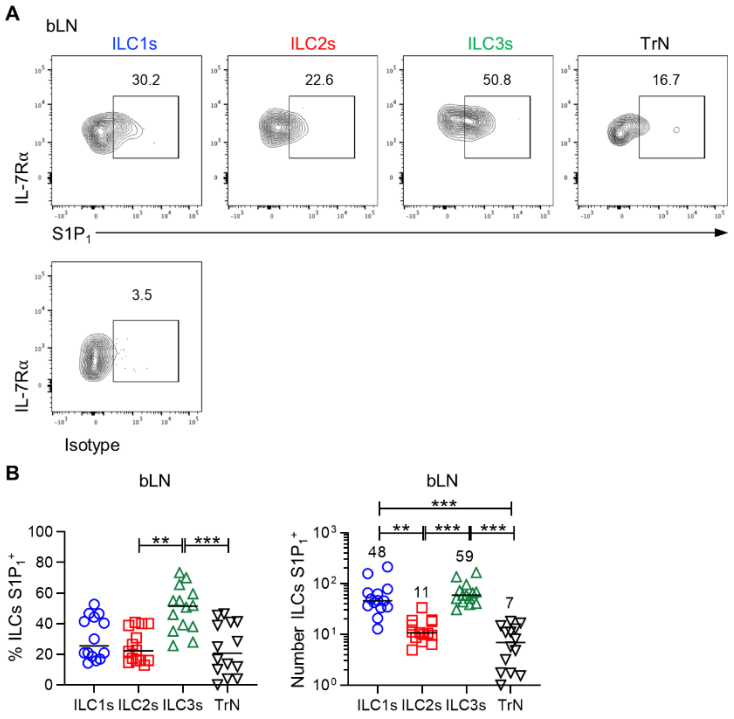

Figure S4. Expression of $S1P_1$ by ILC subsets in the bLN.
To investigate expression of molecules associated with egress from LNs, $S1P_1$ expression was analyzed on all ILC subsets. (**A**) Representative flow cytometry plots showing the expression of $S1P_1$ on ILC1s, ILC2s, ILC3s and triple negative (TrN) cells in the bLN, compared to an isotype control. (**B**) Percentage (left) and total number (right) of ILC subsets expressing $S1P_1$ in the bLN. Data are pooled from 2 independent experiments. Values on flow cytometry plots represent percentages; bars on scatter plots represent the median. Statistical significance was tested using Kruskal-Wallis one-way ANOVA with post hoc Dunn's test: * $p \leq 0.05$, ** $p \leq 0.01$, *** $p \leq 0.005$.

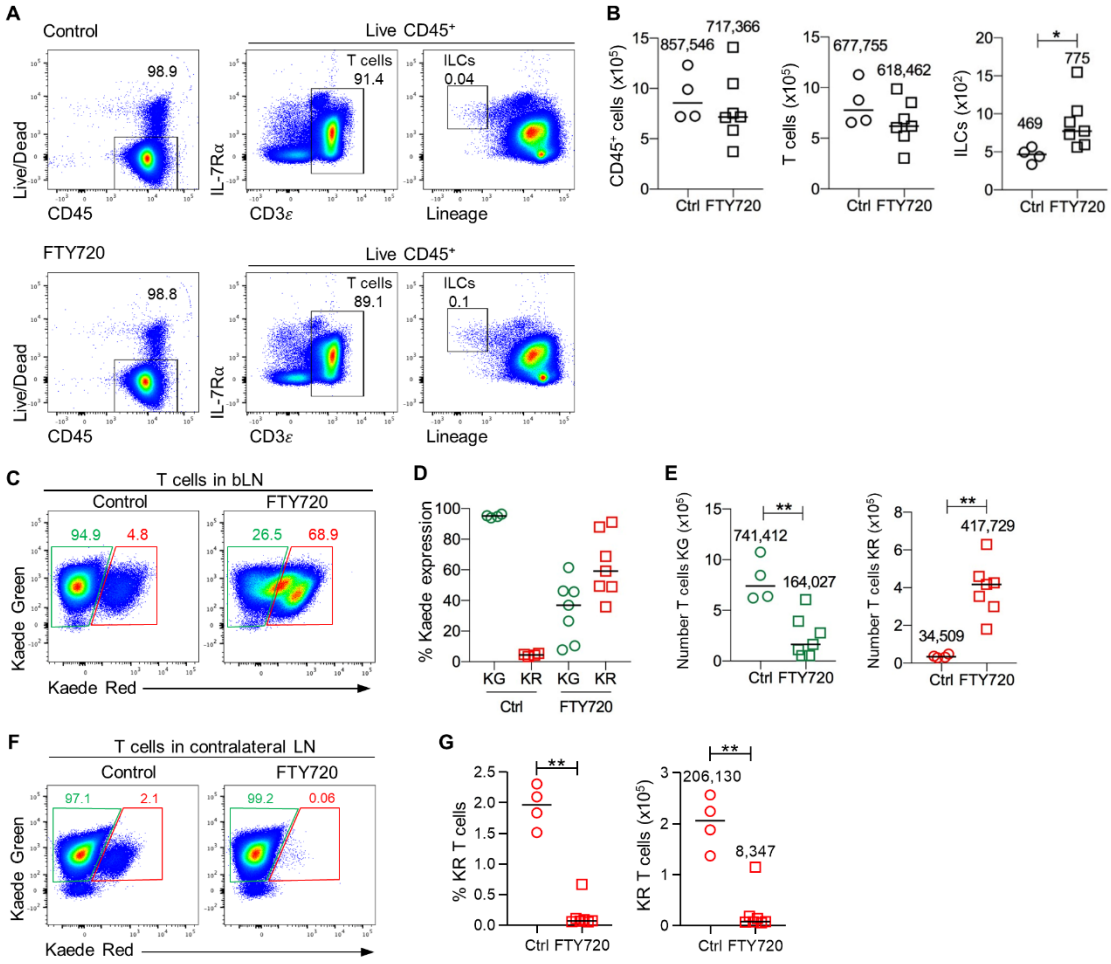

Figure S5. Treatment with FTY720 results in ILC accumulation within the bLN.
To assess the egress of ILCs from peripheral LNs, photoconversion of the bLN of Kaede mice given vehicle control or FTY720 was performed. (**A**) Representative flow cytometry plots showing identification of ILCs and T cells in the bLN. (**B**) Total numbers of CD45$^+$ cells, T cells and ILCs in the bLN at 72 hrs post photoconversion in the presence of the vehicle control (n=4) or FTY720 (n=5).
To confirm the in vivo effects of FTY720 treatment, the T cell compartment was assessed. (**C**) Representative flow cytometry plots showing expression of Kaede Green versus Kaede Red protein by T cells in the bLN 72 hrs after photoconversion. (**D**) Percentage of Kaede Green$^+$ and Kaede Red$^+$ T cells in the bLN of Ctrl (n=4) and FTY720 (n=7) mice. (**E**) Total numbers of Kaede Green$^+$ and Kaede Red$^+$ T cells in the bLN of control (n=4) and FTY720 (n=7) mice. (**F**) Expression of Kaede Green versus Kaede Red by T cells in the contralateral LNs. (**G**) Percentage and total number of Kaede Red$^+$ T cells in the contralateral LNs in the presence of vehicle control (n=5) and FTY720 (n=7). Data are pooled from 2 independent experiments. Values on flow cytometry plots represent percentages; bars on scatter plots represent the median. Statistical significance was tested using an unpaired, non-parametric, Mann-Whitney two-tailed U test: *p≤0.05, **p≤0.01.

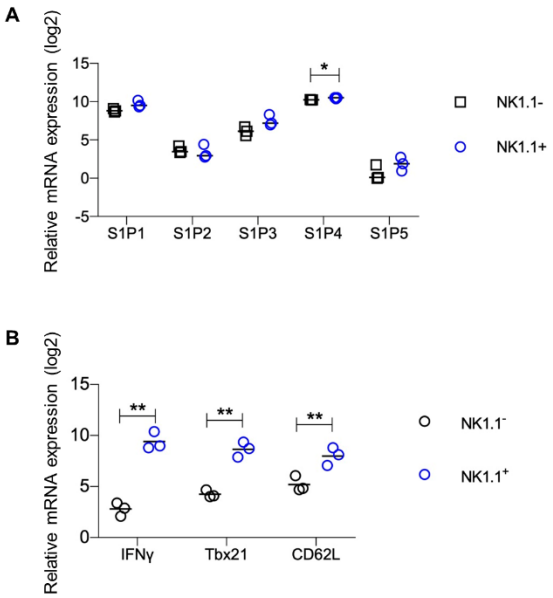

Figure S6. Analysis of S1PR expression by ILCs.
To assess S1PR expression by ILCs in peripheral LNs, (NK1.1^{+}) ILC1s and (NK1.1^{-}) ILCs were isolated by FACS from a pool of peripheral LNs and assessed by qRT-PCR using TaqMan Gene Expression Assays. (**A**) Relative expression of S1PRs by ILC1s versus other ILCs. (**B**) Relative expression of IFN-γ, T-bet, and CD62L by ILC1s versus other ILCs. The mRNA level of each gene was normalized using the mean of three reference genes (18S, GAPDH and β-actin). Statistical significance was evaluated using a paired, parametric, two-tailed U test: *p≤0.05, **p≤0.01.

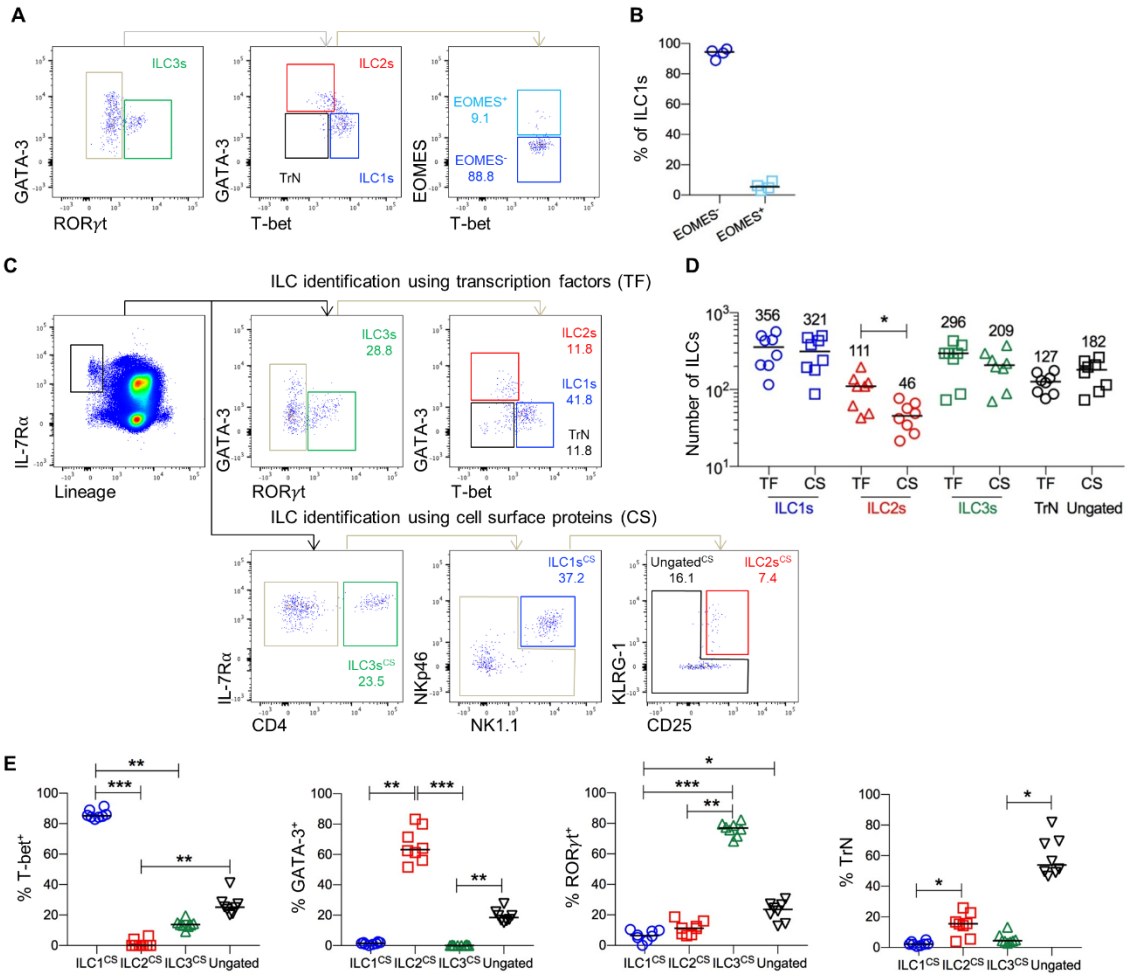

Figure S7. Identification of ILC subsets within the bLN.
To ensure optimal identification of ILC subsets within the LNs of photoconvertible mice, a flow cytometry panel reliant on cell surface markers was validated and compared with subset identification with the transcription factors, GATA-3, RORγt, T-bet and EOMES. When identifying ILCs the following lineage cocktail was used; B220, CD11b, CD11c, CD3, CD5, CD19, Ter119, Gr1, CD49b, F4/80 and FcεRI. (**A**) Flow cytometry plots of ILC subsets within the bLN and EOMES expression on ILC1s. (**B**) Percentage of ILC1s that are EOMES^{+} or EOMES^{-} (n=4).
To identify ILC subsets within the bLN, samples were stained with TF and cell surface markers to identify and validate the gating strategy. (**C**) Flow cytometry plots showing gating strategy used to identify ILC subsets with TF (top) and cell surface (CS) markers (bottom); ILCs identified by CS markers are indicated with a $^{'CS'}$. (**D**) Comparison of numbers of ILC subsets identified by TFs or CS markers (n=8). (**E**) Percentage of T-bet^{+}, GATA-3^{+}, RORγt^{+}, and no TF expression (triple negative; TrN) ILC1s^{CS}, ILC2s^{CS} ILC3s^{CS} and ungated cells (n=7). Each data point represents cells isolated from 1 bLN from one mouse. Data are pooled from a minimum of 2 independent experiments. Bars on scatter plots represent the median, which is also shown numerically. Pairs of samples were compared using a two-tailed Mann-Whitney U test; multiple samples were compared using Kruskal-Wallis one-way ANOVA with post hoc Dunn's test: * $p \leq 0.05$, ** $p \leq 0.01$, *** $p \leq 0.005$.

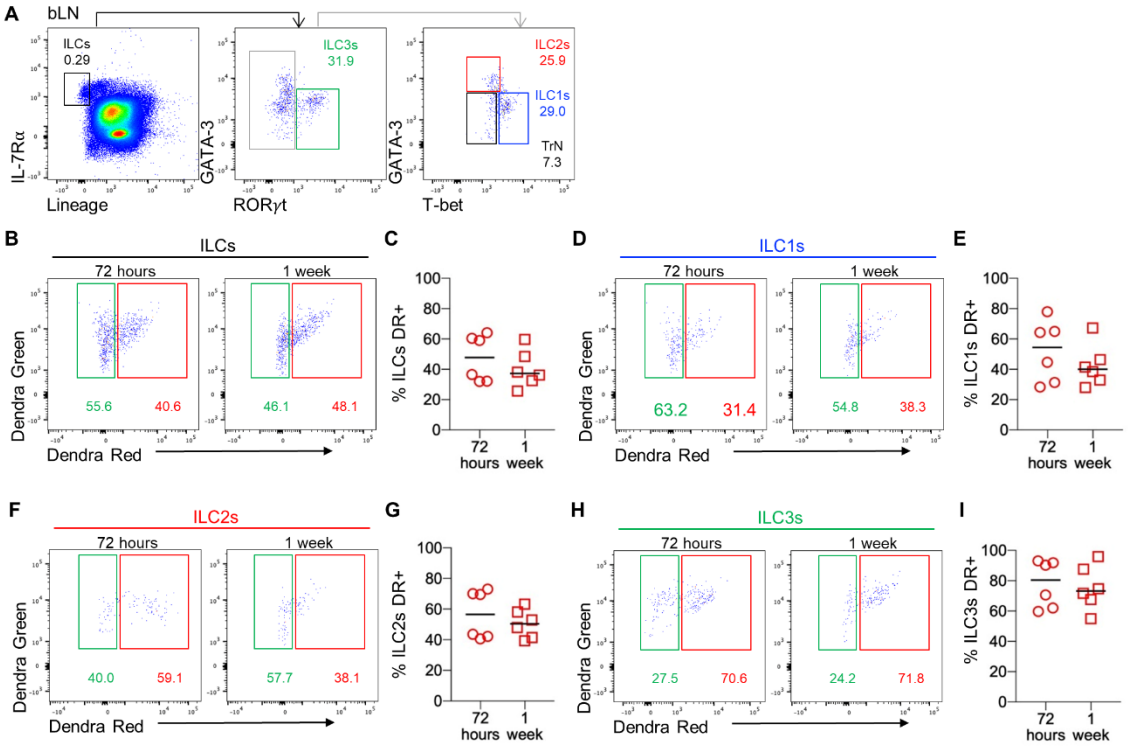

Figure S8. Analysis of ILC residency in LNs using H2B-Dendra2 mice.
To further assess the migratory abilities of the ILC subsets within LNs, photoconversion of the bLN of H2B-Dendra2 mice was performed and mice analyzed at 72 hrs and 1 week post photoconversion. ILC subsets within the bLN ILCs were assessed by expression of the transcription factors GATA-3, RORγt and T-bet. When identifying ILCs the following Lineage cocktail was used; B220, CD11b, CD11c, CD3, CD5, CD19, Ter119, Gr1, CD49b, F4/80 and FcεRI. (**A**) Flow cytometry plots of ILC subsets within the bLN. (**B**) Representative flow cytometry plots of ILC Dendra2 expression post photoconversion. (**C**) Percentage of Dendra2 Red$^+$ (DR$^+$) ILCs within the bLN. (**D**) Representative flow cytometry plots of ILC1 Dendra2 expression post photoconversion. (**E**) Percentage of DR$^+$ ILC1s within the bLN. (**F**) Representative flow cytometry plots of ILC2 Dendra2 expression post photoconversion. (**G**) Percentage of DR$^+$ ILC2s within the bLN. (**H**) Representative flow cytometry plots of ILC3 Dendra2 expression post photoconversion. (**I**) Percentage of DR$^+$ ILC3s within the bLN. Each data point represents cells isolated from 1 bLN from one mouse. Data are pooled from a minimum of 2 independent experiments. Bars on scatter plots represents the median. Samples were compared using Kruskal-Wallis one-way ANOVA with post hoc Dunn's test: * $p \leq 0.05$, ** $p \leq 0.01$, *** $p \leq 0.005$.

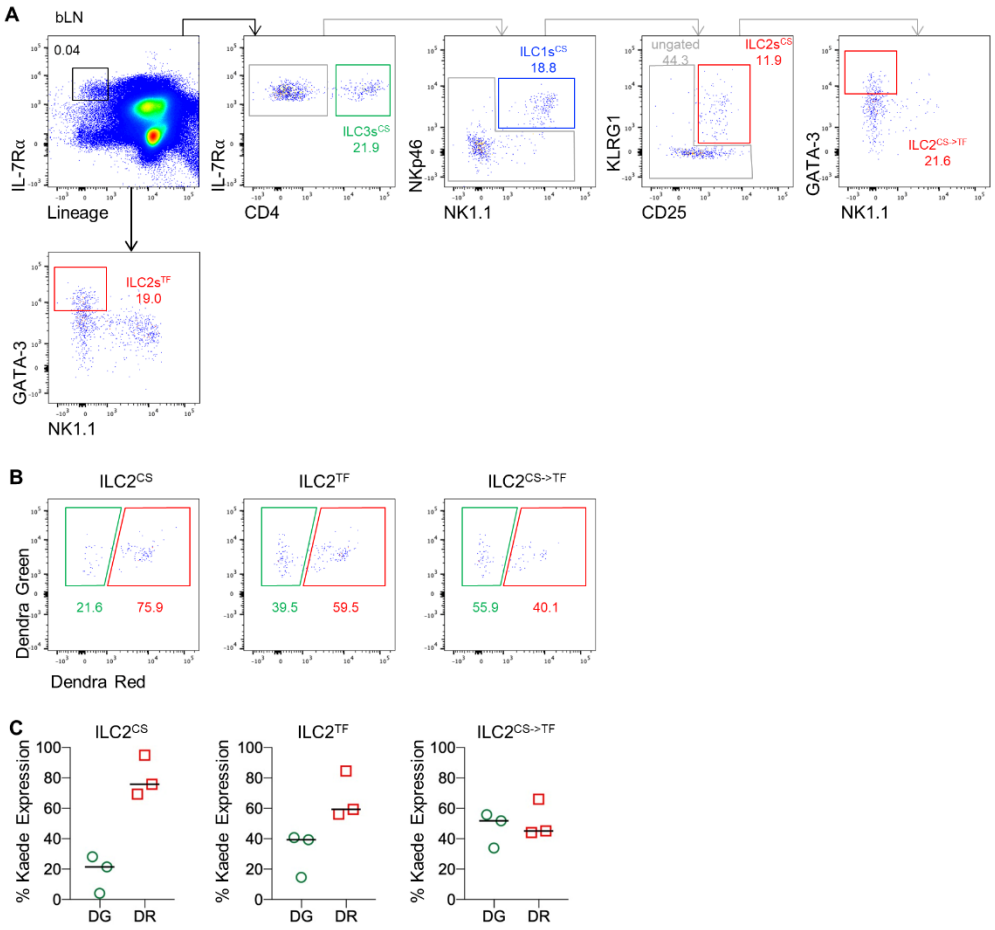

Figure S9. Differences in Dendra Red expression by ILC2 dependent upon identification by transcription factor or cell surface marker expression.
To compare the differences between the migratory properties of ILC2s identified by cell surface (CS) markers or by transcription factors (TF), the bLN of H2B-Dendra2 mice was photoconverted and assessed 72 hrs later. When identifying ILCs the following lineage cocktail was used; B220, CD11b, CD11c, CD3, CD5, CD19, Ter119, Gr1, CD49b, F4/80 and FcεRI. (**A**) Representative flow cytometry plots identifying ILC2s via CS markers ($ILC2^{CS}$) (IL-7Rα$^+$ Lineage$^-$ CD4$^-$ (NK1.1$^+$ NKp46$^+$)$^-$ (KLRG1$^+$ CD25$^+$)$^+$), ILC2s via TF ($ILC2s^{TF}$) (IL-7Rα$^+$ lineage$^-$ GATA-3$^+$) and ILC2s within the ungated fraction of the CS marker gating via TFs ($ILC2^{CS->TF}$) (IL-7Rα$^+$ Lineage$^-$ CD4$^-$ (NK1.1$^+$ NKp46$^+$)$^-$ (KLRG1$^+$ CD25$^+$)$^-$ GATA-3$^+$). (**B**) Representative flow cytometry plots showing Dendra Green and Dendra Red expression of $ILC2^{CS}$, $ILC2^{TF}$ and $ILC2^{CD->TF}$. (**C**) Dendra expression of $ILC2^{CS}$, $ILC2^{TF}$ and $ILC2^{CS->TF}$. Each data point represents cells isolated from 1 bLN from one mouse. Bars on scatter plots represent the median.

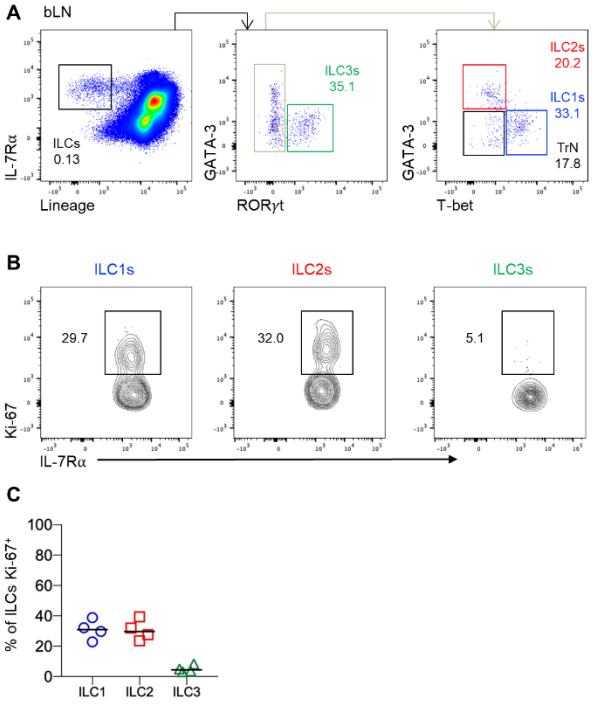

Figure S10. Expression of Ki-67 by ILC subsets within the bLN.
To investigate proliferation rates amongst ILC subsets within the bLN, expression of Ki-67 was analyzed. When identifying ILCs the following lineage cocktail was used; B220, CD11b, CD11c, CD3, CD5, CD19, Ter119, Gr1, CD49b, F4/80 and FcεRI. (**A**) Flow cytometry plots of ILC subsets within the bLN, cells first gated on live CD45$^+$ cells. (**B**) Flow cytometry plots showing representative Ki-67 expression by ILC1s, ILC2s, ILC3s. (**C**) Percentage Ki-67 expression by ILC1s, ILC2s and ILC3s (n=4). Data are representative of 2 independent experiments. Bars on scatter plots represent the median.

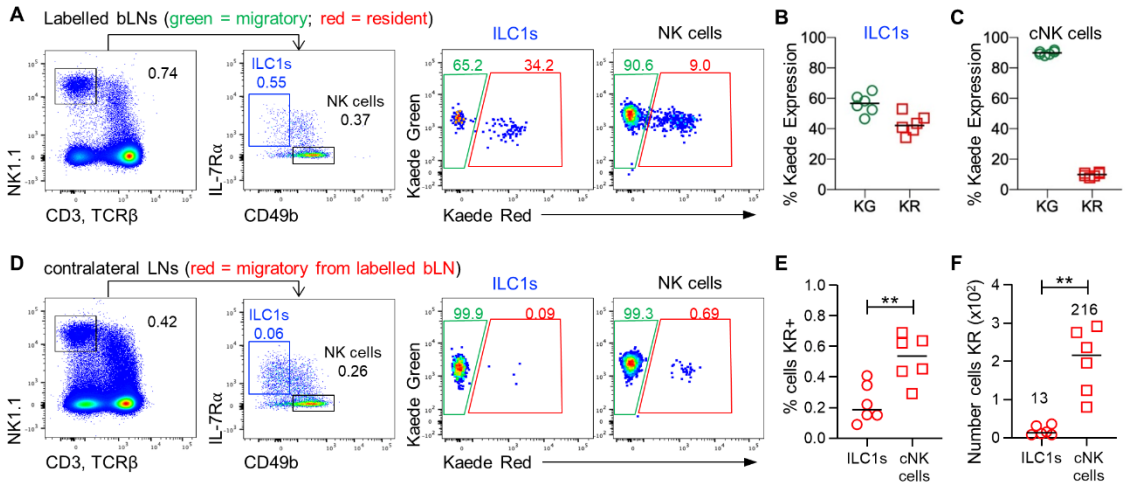

Figure S11. Comparison of ILC1 and NK cell recirculation through peripheral lymph nodes.

The ability of ILC1s to recirculate through peripheral LNs was compared with that of NK cells. The bLN was photoconverted and then assessed, alongside contralateral peripheral LNs 72 hrs later. (**A**) Representative flow cytometry plots showing identification of ILC1s and NK cells in the labelled bLN and their expression of Kaede Red versus Kaede Green protein. (**B**) The percentage of ILC1s expressing Kaede Red or Kaede Green. (**C**) Percentage of NK cells expressing Kaede Red or Kaede Green. (**D**) Representative flow cytometry plots showing identification of ILC1s and NK cells in contralateral LNs and their expression of Kaede Red versus Kaede Green protein. (**E**) Percentage of NK cells and ILC1s expressing Kaede Red protein in contralateral LNs. (**F**) Total number of NK cells and ILC1s expressing Kaede Red protein in contralateral LNs. Data (n=6) from 1 independent experiment. Values on flow cytometry plots represent percentages; bars on scatter plots represent the median, which is also shown numerically. Statistical significance was tested using an unpaired, non-parametric, Mann-Whitney two-tailed U test: *p≤0.05, **p≤0.01.

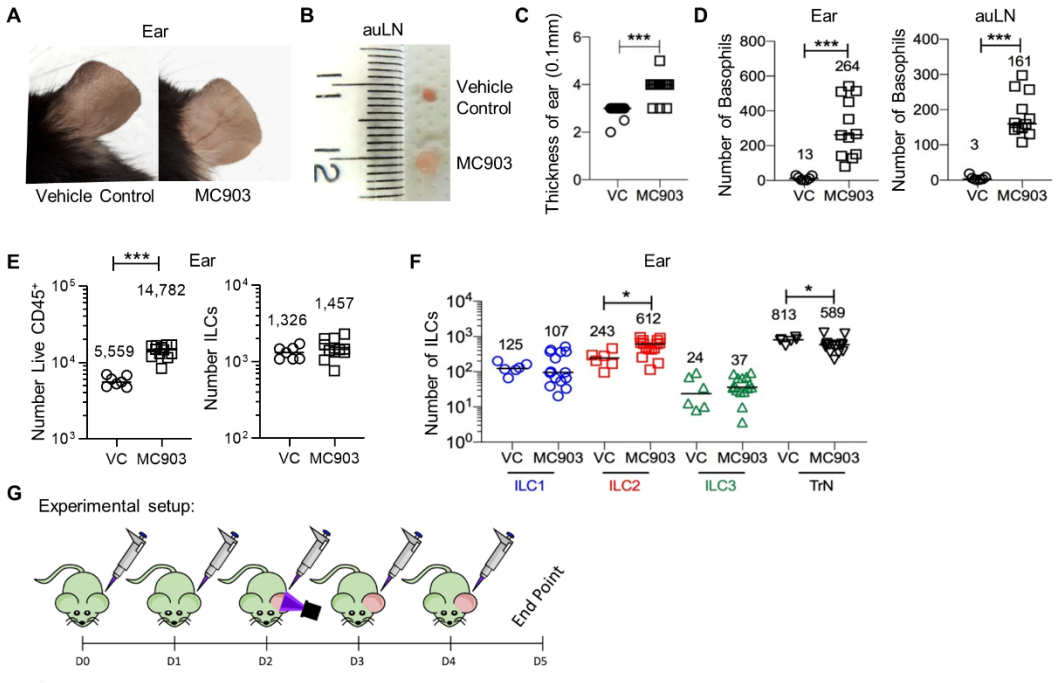

Figure S12. Induction of atopic dermatitis causes an increase in the frequency of ILC2 in ear skin.

To investigate the potential migration of ILCs from inflamed skin to the draining auLN, MC903 was applied to the ears of WT mice for 5 consecutive days to induce atopic dermatitis. (**A**) Ears of mice after application of the vehicle control (VC) (left) or MC903 (right) on the ear. (**B**) auLN of mice after application of the VC (top) or MC903 (bottom) on the ear. (**C**) Thickness of the ear skin of mice treated with VC or MC903. (**D**) Total number of basophils in the ear and auLN of mice treated with vehicle control (VC, n=7) or MC903 (n=12). (**E**) The number of $CD45^+$ cells and ILCs in the ear of mice treated with vehicle control (VC, n=7) or MC903 (n=12). (**F**) Total number of different ILC subsets in the ear of mice treated with vehicle control (VC, n=6) or MC903 (n=15). (**G**) Schematic showing the experimental design of MC903 treatment combined within photoconversion of the inflamed ear. Data are pooled from a minimum of 2 independent experiments. Each data point represents cells isolated from 1 ear and 1 auLN. Bars on scatter plots represent the median, which is also shown numerically. Statistical significance was tested using an unpaired, non-parametric, Mann-Whitney two-tailed U test: *p≤0.05, **p≤0.01, ***p≤0.001.

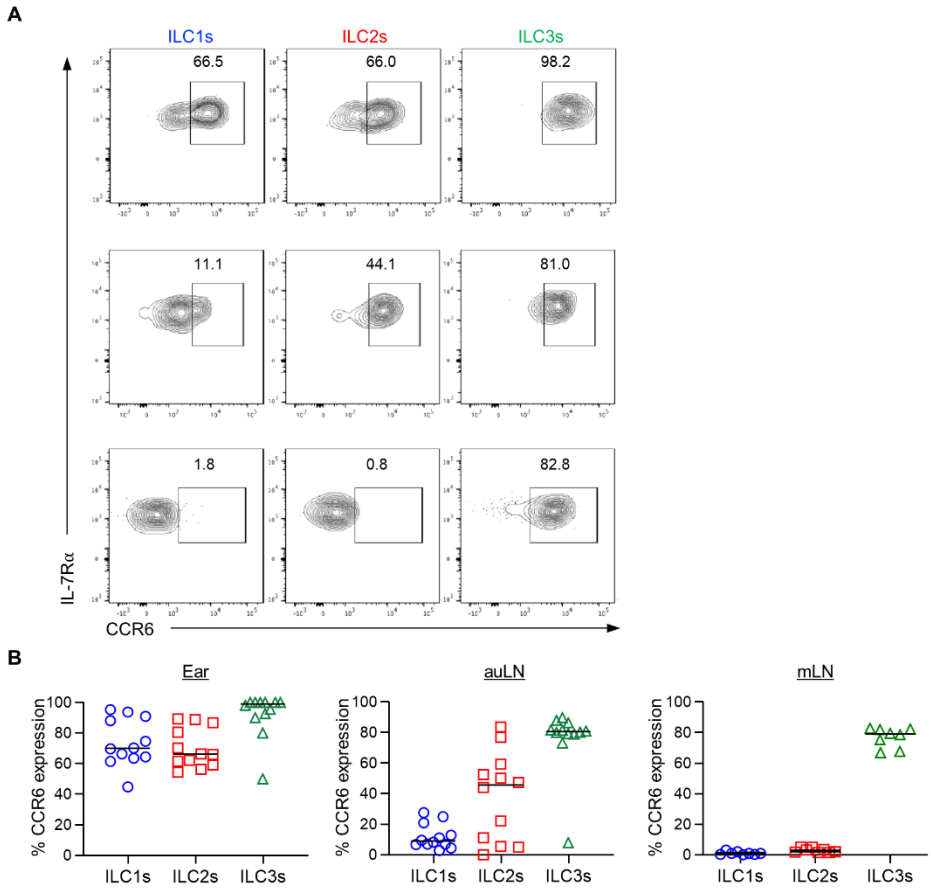

Figure S13. CCR6 is expressed by all ILC subsets in the ear and auLN.
CCR6 expression by ILCs isolated from skin, peripheral LNs and mLN were compared using flow cytometry. ILCs were identified as CD45$^+$IL-7Rα$^+$Lin{B220, CD11b, CD11c, CD3, CD5, CD19, Ter119, Gr1, CD49b, F4/80, FcεRI}$^-$ cells with subsets identified based upon transcription factor expression. (**A**) Representative flow cytometry plots of CCR6 expression by ILC1s, ILC2s and ILC3s isolated from the ear, auLN and mLN. (**B**) Percentage of ILC1s, ILC2s and ILC3s expressing CCR6 within the ear (left) (n=12), auLN (middle) (n=12) and mLN (right) (n=8). Each data point represents cells isolated from 1 ear, 1 auLN and 1 whole mLN. Data are pooled from a minimum of 2 independent experiments. Values on flow cytometry plots represent percentages; bars on scatter plots represent the median.